ACS Partner Journal

Journal of the American Society for Mass Spectrometry

pubs.acs.org/jasms

Research Article

Radical Cascade Dissociation Pathways to Unusual Nucleobase Cation Radicals

Václav Zima, Yue Liu, and František Tureček*

Cite This: *J. Am. Soc. Mass Spectrom.* 2022, 33, 1038−1047

Read Online

ACCESS | Metrics & More | Article Recommendations | Supporting Information

ABSTRACT: We report unusual dissociations of protonated RNA nucleosides tagged with radical initiator groups at ribose 5′-O and furnished with a 2′,3′-*O*-isopropylidene protecting group. The ions undergo collision-induced radical cascade dissociations starting at the radical initiator that break down the dioxolane ring and trigger the formation of nucleobase cations and cation radicals. The adenine cation radical that was formed by radical cascade dissociations was identified by MS^5 UV−vis photodissociation action spectroscopy to be a higher-energy N-3-H tautomer of the canonical ionized nucleobase. The guanine cation radical was formed by radical cascade dissociations as the N-7-H tautomer. In contrast to adenosine and guanosine, radical cascade dissociations of the tagged ribocytidine ion produced protonated cytosine, whereas tagged ribothymidine showed yet different dissociations resulting in predominant thymine loss. Reaction mechanisms were suggested for the cascade dissociations that were based on Born−Oppenheimer molecular dynamics and density functional theory calculations that were used to map the relevant parts of the potential energy surfaces for adenosine, guanosine, and cytidine radical ions. The reported radical cascade dissociations represent a new, nonredox approach to nucleobase and nucleoside cation radicals that has the potential of being expanded to the generation of various oligonucleotide cation radicals.

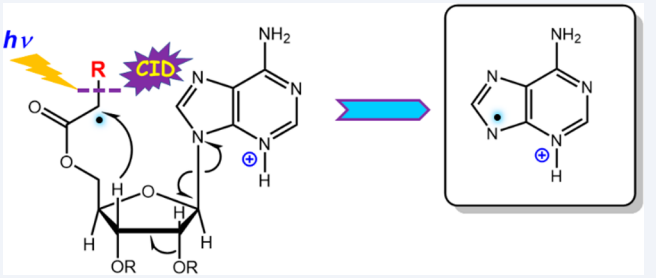

INTRODUCTION

DNA ionization is known to proceed along oxidative and reductive pathways, forming respectively cation-radical and anion-radical intermediates that lead to different radical products.[1] Oxidative ionization by electron removal produces transient cation radicals that can react further by electron or proton transfer.[2−5] Reductive ionization involves capture of a slow secondary electron, forming transient anion radicals that are converted to radicals by anion elimination or protonation by solvent.[6] Despite extensive research of DNA ionization, structure characterization of highly reactive cation-radical intermediates remains challenging.[3] Recent studies have indicated that DNA-related cation radicals, such as nucleobases, nucleosides, and oligonucleotides, can be generated in the gas phase, isolated by mass, and studied by tandem mass spectrometry in combination with action spectroscopy in the infrared or UV−visible regions.[7] This technique relies on wavelength-dependent photodissociation whereby the photofragment ion production is used to reconstruct the absorption profile of the isolated ion.[8] When combined with analysis of theoretical vibrational or vibronic absorption spectra, action spectroscopy allows structural assignment to be made for the cation radicals generated in the gas phase. The generation and structure elucidation of gas-phase cation radicals related to nucleic acid components have been successfully accomplished for several standard and modified nucleobases using intramolecular electron transfer in complexes with Cu^{II} and a coligand, such as terpyridine, in which nucleobase oxidation by Cu^{II} was driven by collision-induced dissociation (CID, Scheme 1, eq 1).[9,10] This oxidative pathway technique, that has been introduced by O'Hair and co-workers,[9,10] has been shown to work for the formation of cation radicals of the four

Scheme 1. Formation of Nucleobase, Nucleoside, and Nucleotide Cation Radicals in the Gas Phase

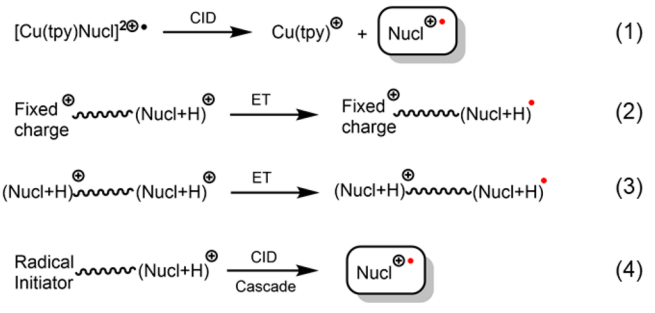

Received: April 3, 2022
Revised: April 28, 2022
Accepted: May 2, 2022
Published: May 10, 2022

https://doi.org/10.1021/jasms.2c00098
J. Am. Soc. Mass Spectrom. 2022, 33, 1038−1047

standard DNA nucleobases,[9,10] as well as for synthetic analogues of the hachimoji type.[11] However, oxidative generation of nucleoside and nucleotide cation radicals has so far been limited to 2′-deoxyguanosine and guanosine.[12,13] The reductive pathway to nucleoside and nucleotide cation radicals that mimic products of reductive DNA ionization relies on partial reduction by electron transfer (ET) of dications represented as derivatives furnished with a fixed-charge group (Scheme 1, eq 2),[14] or multiply charged oligonucleotide ions (Scheme 1, eq 3).[15,16] We now report a new, nonredox approach to the generation of nucleobase cation radicals that has the potential of being extended to nucleoside and nucleotide cation radicals. The new methodology relies on the uncoupled generation of the charged and radical-carrying moieties in a nucleoside conjugate (Scheme 1, eq 4). Charging is achieved by electrospray ionization to protonate the most basic position in the nucleobase. The radical is generated from a mass-selected ion by CID of an auxiliary and covalently attached group denoted as Radical Initiator in eq 4. For this study, we chose the standard 4,4′-azobis(4-cyanovaleric acid) (ABCV) group that was tethered as an ester to 5′-*O* of protected ribose (Figure 1).

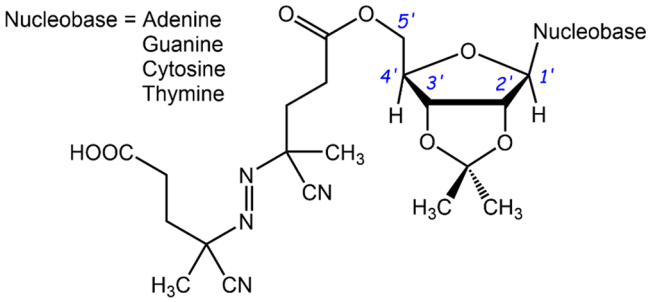

Figure 1. Ribonucleoside conjugates tagged with the ABCV radical initiator.

We note that ABCV and other radical initiators have been used previously to form peptide and carbohydrate radical ions and promote their fragmentation.[17,18] Here we show that radical-triggered dissociations of protonated tagged ribonucleosides form unexpected products that can be characterized by action spectroscopy in combination with density functional theory (DFT) calculations to assign gas-phase ion structures.

EXPERIMENTAL SECTION

Materials and Methods. Ribonucleoside conjugates were synthesized and characterized as described in detail in the Supporting Information (Schemes S1−S4). Starting materials were purchased from Sigma-Aldrich, Fisher Chemical, St. Louis, MO) and used as received. Acetonitrile was dried using 4A molecular sieves, grade 514 (8−12 mesh). Chromatography was performed on Acros Organics silica gel, ultrapure, 60−200 μm, 60A. TLC was performed on TLC silica gel 60 F_{254} aluminum sheets. Spots were detected with permanganate stains, with bromocresol green stains, or under a UV lamp. ^{1}H NMR spectra were recorded on Bruker spectrometers at 300 and 500 MHz. ^{13}C NMR Spectra were recorded at 126 MHz. Coupling constants (*J*) are given in hertz (Hz) and chemical shifts are on the δ-scale (Figures S1−S32, Supporting Information). NMR characterization was carried out according to the atom numbering shown in Scheme S1 (Supporting Information). High resolution mass spectra were recorded on an LTQ-Orbitrap XL (ThermoElectron, San Jose, CA) at 60 000 resolution. Samples were introduced by flow injection into the ESI source. Action spectroscopy measurements were performed on a modified Bruker amaZon (Bruker Daltonik, Bremen, Germany) ion trap mass spectrometer equipped with an auxiliary ion source for electron transfer dissociation (ETD) and coupled to a Nd:YAG laser/OPO laser system.[19] The synthetic conjugates were dissolved in 50:50:1 acetonitrile−water−acetic acid at 10−20 μM concentrations and electrosprayed into the ion trap. Singly charged conjugate ions were selected by mass and subjected to multistep collision-induced dissociations. The nucleobase cation radicals formed were again selected by mass in the ion trap and probed by laser photodissociation. The laser beam was provided by an EKSPLA NL301G Nd:YAG laser (Altos Photonics, Bozeman, MT) working at 20 Hz frequency and 3 to 6 ns pulse width. The photon pulses were treated by a PG142C unit (AltosPhotonics) which incorporated a third harmonic generator and optical parametric oscillator coupled with an optional second harmonic generator to enable wavelength tuning in the range of 210−700 nm. The laser beam (6 mm diameter) exiting the PG142C unit was aligned and focused into the ion trap. The laser pulse energies were measured at each experimental wavelength using an EnergyMax-USB J-10MB energy sensor (Coherent Inc., Santa Clara, CA) to calibrate the action spectra. The measured photofragment ion intensities were normalized to the number of photons per pulse.

Calculations. Calculations were performed according to the multistep protocol that had been developed previously.[20] Briefly, in the first step, several conformers were constructed for each cation-radical protomer where the additional hydrogen atom was placed in the adenine (N-1, N-3, or N-7), guanine (N-7, O-6), cytosine (O-2, N-3), and thymine (O-4, O-2) positions. A conformation search of the cation-radical structures was performed by Born−Oppenheimer molecular dynamics calculations (BOMD) using the Berendsen thermostat algorithm[21] at 310 K. BOMD trajectories were run for 20 ps with 1 fs steps using the all-valence-electron semiempirical PM6-D3H4 method[22] that includes corrections for hydrogen bond and dispersion energies. These calculations were run by MOPAC[23] under the Cuby4 platform.[24] This generated 20 000 snapshots from each trajectory from which 200 × *n* (*n* = number of trajectories) structures were selected at regular intervals and gradient-optimized with PM6-D3H4. The optimized structures for each protomer were ranked by energy, and the sets were compacted by removing duplicates. Gradient optimization of these second-selection structures was carried out with the B3LYP hybrid density functional[25] in the spin-unrestricted format and the 6-31+G(d,p) basis set. This provided several structures for each protomer that were characterized by harmonic frequency calculations as local energy minima. B3LYP structures within 40 kJ mol^{-1} of each protomer group energy minimum were then reoptimized with M06-2X[26] using the 6-31+G(d,p) basis set including harmonic vibrational analysis. These standard density functional theory (DFT) calculations were run with the Gaussian 16 program suite (Revision A01).[27] We selected the B3LYP/6-31+G(d,p) harmonic frequencies, scaled by 0.975, to evaluate the zero-point energies and vibrational enthalpy and entropy terms. This was guided by the known reliability of scaled B3LYP/6-31+G(d,p) harmonic frequencies to provide a good match with frequencies measured in infrared action spectra in the gas

https://doi.org/10.1021/jasms.2c00098
J. Am. Soc. Mass Spectrom. 2022, 33, 1038−1047

phase.[28] For single-point energy calculations, we used the M06-2X/6-31+G(d,p)-optimized geometries. This is natural for M06-2X/6-311++G(2d,p) single-point energy calculations, where triple-ζ quality basis sets improve accuracy and were used by Zhao and Truhlar to benchmark the density functional.[26] On the basis of our previous benchmarks,[11,13,14] we selected time-dependent density functional theory calculations[29] with UM06-2X/6-31+G(d,p) of an extensive set of vertical and vibronic transitions in the cation radicals. Vertical excitations were calculated for 45−50 excited states to probe transitions within the experimentally studied region of 210−700 nm. To calculate vibronic excitations, we used 300 Boltzmann-ranked Wigner configurations[30,31] that were generated by the Newton X program[32] from the B3LYP/6-31+G(d,p) calculated harmonic normal modes of each cation radical at 350 K and submitted for TD-DFT calculations. The number of excited electronic states in these vibronic TD-DFT calculations (25) was chosen to include excitations with wavelengths down to below 200 nm, covering a large part of the experimental wavelength range of 210−700 nm. Transition states (TS) were located by stepwise B3LYP and M06-2X calculations to map the potential energy surface along the reaction coordinate. The TS were characterized by harmonic frequency analysis as having one imaginary frequency.

RESULTS AND DISCUSSION

Radical Cascade Dissociations of Adenosine Conjugates and Formation of Adenine Cation Radicals. Electrospray ionization of the ribonucleoside conjugates produced singly charged ions that were selected by mass and subjected to CID. Starting with the adenosine ABCV conjugate CID-MS^2 of cation $\mathbf{1}^+$ (m/z 570) resulted in the combined loss of N_2 and 2-methylglutaronitrile radical, forming the m/z 416 radical ion (Figure 2a) that was selected and subjected to CID-MS^3. Dissociation of this intermediate proceeded by a consecutive elimination of 2-methylprop-2-enenitrile (67 Da) and acetone (58 Da) from the dioxolane ring, forming the respective radical ions at m/z 349 and m/z 291 (Figure 2b). Rather unexpectedly, the dissociation proceeded even further by loss of the entire deoxyribose moiety, forming the adenine cation radical $\mathbf{A}^{+\bullet}$ at m/z 135. All these fragment ions were assigned by accurate mass measurements. The highest yield of $\mathbf{A}^{+\bullet}$ was obtained by CID-MS^4 of the isolated m/z 291 intermediate where it was the only major product that was formed by the elimination of the neutral 5′-*O*-acetyldeoxyribose ($C_7H_8O_4$) molecule (Figure 2c). This last dissociation step was critically linked to the presence of the 2′,3′-*O*-isopropylidene group in $\mathbf{1}^+$ and m/z 349 reaction intermediates. This was probed by CID-MS^n spectra of protonated conjugate $\mathbf{1b}^+$ in which the 2′-OH and 3′-OH groups were deprotected. CID-MS^2 of $\mathbf{1b}^+$ (m/z 530) showed radical dissociations of the ABCV side chain, yielding successively fragment ions at m/z 376 by loss of N_2 and 2-methylglutaronitrile radical (Figure 3a), and m/z 309 by loss of 2-methylprop-2-enenitrile (Figure 3b). Thus, the dissociations of the radical initiator group in $\mathbf{1b}^+$ were completely analogous to those starting from $\mathbf{1}^+$. However, subsequent CID of the m/z 309 intermediate predominantly resulted in a ribose cross-ring cleavage, forming an even-electron fragment ion at m/z 163 (Figure 3c). Ion $\mathbf{A}^{+\bullet}$ at m/z 135 was also formed, but only as a very minor product, whereas most of the adenine ions were protonated (m/z 136).

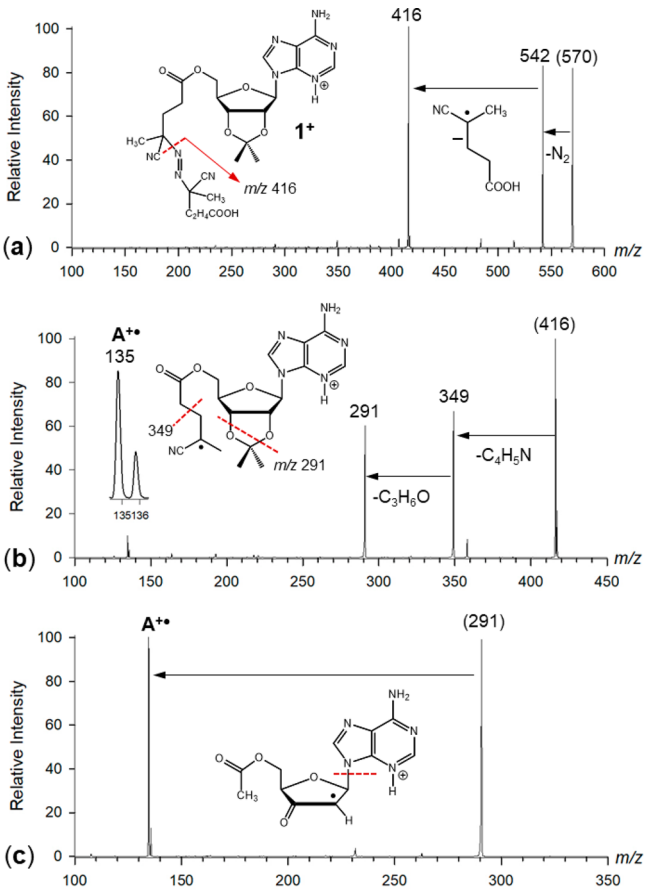

Figure 2. Collision-induced dissociation mass spectra of (a) $\mathbf{1}^+$, (b) m/z 416, and (c) m/z 291 cation-radical intermediates showing the formation of $\mathbf{A}^{+\bullet}$.

As a next step in elucidating these ion dissociations, we isolated ion $\mathbf{A}^{+\bullet}$ and investigated it by MS^5 UV−vis photodissociation action spectroscopy by monitoring photofragment ion channels for the major loss of HCN (m/z 108), and a minor loss of two HCN (m/z 81). We note that to the best of our knowledge these are the first MS^5 ion photodissociation spectra ever reported. The spectra showed two major absorption bands with maxima at 515 and 340 nm, as well as shoulders or maxima at 300, 270, 230, and 220 nm (Figure 4a). A D_3-labeled derivative, $C_5H_2D_3N_5^{+\bullet}$, was generated following H/D exchange of the adenine labile protons, and its UV−vis action spectrum is shown in Figure 4b. The dissociations leading to the absorption band at 515 nm displayed equal contributions from the loss of HCN and DCN (Figure 4b). In contrast, the 340 nm band was composed of a major band for DCN loss that had a maximum at 340 nm, and a minor band for HCN loss with a maximum at 320 nm. The relative intensities of these two distinct bands did not reflect the 3:2 ratio of D and H in the ion, which along with the different band maxima indicated distinct mechanisms for the hydrogen cyanide eliminations.

The action spectrum of $\mathbf{A}^{+\bullet}$ was assigned on the basis of the vibronic absorption spectra of several adenine cation-radical tautomers that were calculated by time-dependent DFT.[33,34] The best match was obtained for the N3−H tautomer $\mathbf{A1}^{+\bullet}$ which showed a prominent band for excitation to the F state and a broad band in the visible region of the spectrum for excitations to the C and D states (Figure 4c). Several other

https://doi.org/10.1021/jasms.2c00098
J. Am. Soc. Mass Spectrom. 2022, 33, 1038−1047

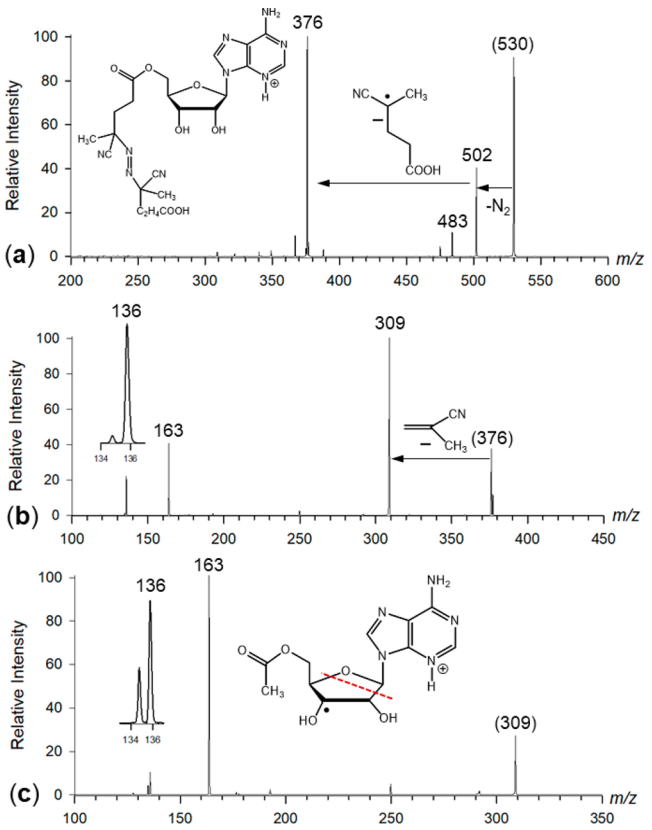

Figure 3. (a) CID-MS^2 spectrum of protonated adenosine conjugate **1b** at m/z 530. (b) CID-MS^3 spectrum of fragment ion at m/z 376. (c) CID-MS^4 spectrum of fragment ion at m/z 309. Insets show the $(\mathbf{A} + \mathrm{H})^+$ and $\mathbf{A}^{+\bullet}$ ion profiles at m/z 136 and 135, respectively.

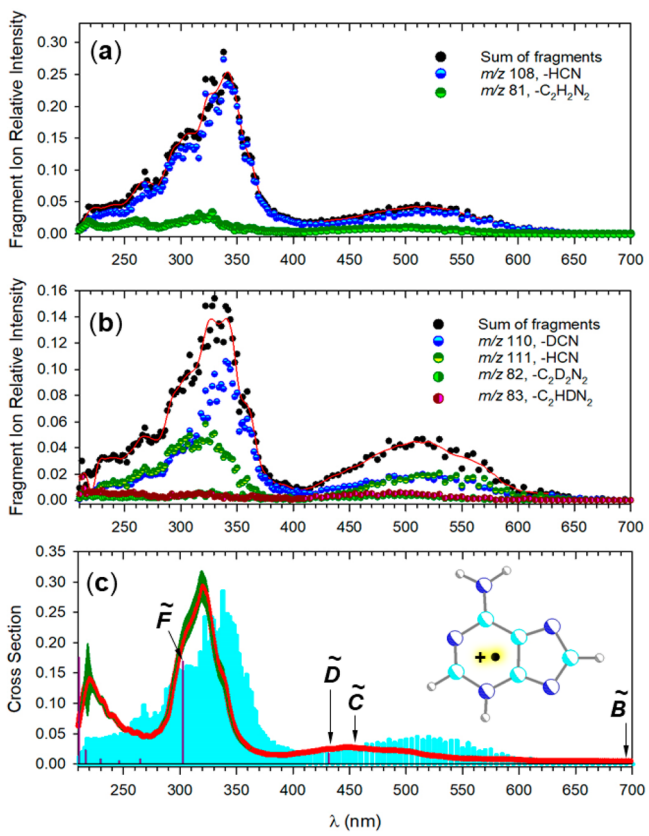

Figure 4. UV−vis action spectra of (a) $\mathbf{A}^{+\bullet}$ and (b) $[D_3]\mathbf{A}^{+\bullet}$. (c) Red line: time-dependent DFT M06-2X/6-31+G(d,p) calculated vibronic spectrum of $\mathbf{A1}^{+\bullet}$ from 300 configurations at 350 K. The vertical lines indicate TD-DFT electron transitions. The action spectrum is shown as cyan background.

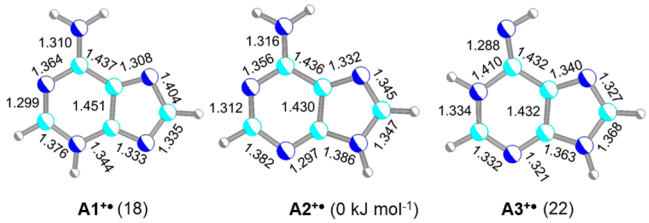

Figure 5. M06-2X/6-31+G(d,p)-optimized structures of the three lowest-energy adenine cation radical tautomers. Bond lengths are in angstroms. In parentheses are relative CCSD(T)/CBS + zero-point energies in kJ mol^{-1} referring to 0 K.

adenine ion isomers (Figure 5) were excluded, because their calculated vibronic spectra showed major bands that were absent in the action spectrum of $\mathbf{A}^{+\bullet}$.[33] Previous ab initio calculations with CCSD(T) that were extended to the complete basis set[33] have indicated that $\mathbf{A1}^{+\bullet}$ was the second lowest-energy tautomer among adenine cation radicals, being 18 kJ mol^{-1} higher by energy than the canonical N9−H isomer ($\mathbf{A2}^{+\bullet}$) and 4 kJ mol^{-1} lower than the N1-H,N6-imine isomer $\mathbf{A3}^{+\bullet}$. The action spectrum of $\mathbf{A2}^{+\bullet}$ that has been reported previously showed a band with a maximum at 290 nm, which coincided with the shoulder at 300 nm in the spectrum of $\mathbf{A1}^{+\bullet}$. Although a shoulder was also predicted to belong to $\mathbf{A1}^{+\bullet}$ according to the calculated vibronic spectrum (Figure 4c), a minor presence of the most stable $\mathbf{A2}^{+\bullet}$ isomer in the spectrum of $\mathbf{A}^{+\bullet}$ cannot be excluded. Similarly, the calculated absorption spectrum of isomer $\mathbf{A3}^{+\bullet}$ showed a strong band with a maximum at 240 nm[33] which was absent in the action spectrum of $\mathbf{A}^{+\bullet}$.

Mechanism of Adenine Cation-Radical Formation. The unexpected formation of $\mathbf{A1}^{+\bullet}$ from the adenosine−ABCV conjugate raised the question of the reaction mechanism. The conjugate was designed with the intention to undergo a cascade dissociation of the ABCV chain to generate a reactive 5′-*O*-acetyl radical ($\mathbf{2}^{+\bullet}$) which was presumed to be quenched by a tertiary hydrogen migration from a ribose position (Scheme 2). We used density functional theory calculations with M06-2X/6-311++G(2d,p) to establish the ion structures, map the potential-energy surface, and locate transition states (TS) for H atom migrations to the 5′-*O*-acetyl radical from the

Scheme 2. Ribose 3′-Hydrogen Atom Migration in 5′-*O*-Acetoxyadenosine Radical Intermediate $\mathbf{2}^{+\bullet}$[a]

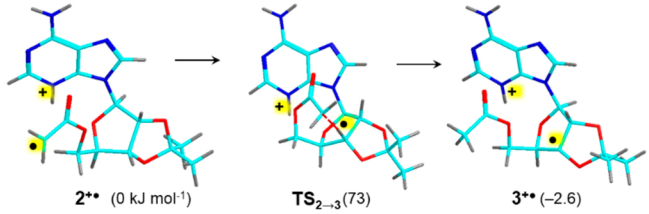

[a]Atom color coding: cyan = C, red = O, blue = N, gray = H. Relative energies in parentheses are from M06-2X/6-311++G(2d,p) calculations including zero-point vibrational energies and referring to 0 K.

https://doi.org/10.1021/jasms.2c00098
J. Am. Soc. Mass Spectrom. 2022, 33, 1038−1047

sterically accessible ribose positions. We note that adenine protonation at N3 in conjugate **1** was calculated to be energetically preferred over protonation at N1 and N7, consistent with previous studies of gas-phase adenosine ions by Rodgers and co-workers.[35] The TS energies for H atom migration in $\mathbf{2}^{+\bullet}$ from C5′, C4′, C3′, and C2′, E_{TS} = 108, 129, 73, and 100 kJ mol^{-1}, respectively, pointed to a kinetic preference for the migration of C3′-H, forming the C3′ radical $\mathbf{3}^{+\bullet}$ (Scheme 2). All these H migrations were exergonic, forming isomeric ribose radicals $\mathbf{4}^{+\bullet}$–$\mathbf{6}^{+\bullet}$ (Scheme S5–S7, Supporting Information) and indicating the possibility of spontaneous isomerization.

It should be noted that radical $\mathbf{3}^{+\bullet}$ that was produced by the kinetically most favorable migration via $\mathbf{TS}_{2\rightarrow3}$ was not the lowest-energy isomer. The further reaction course leading to $\mathbf{A1}^{+\bullet}$ involved radical-induced cleavage of the dioxolane ring in $\mathbf{3}^{+\bullet}$ via $\mathbf{TS}_{3\rightarrow7}$ and elimination of acetone, forming ion $\mathbf{7}^{+\bullet}$ with a radical-activated C1′–N9 bond (Scheme 3). The final

Scheme 3. Ribose Dissociations Forming Ion $\mathbf{A1}^{+\bullet}$[a]

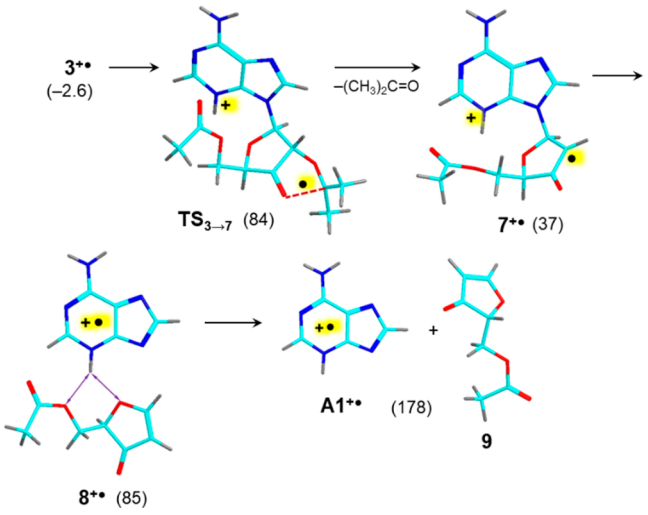

[a]Structure and energy description as in Scheme 2.

dissociation of $\mathbf{7}^{+\bullet}$ may proceed via an ion–molecule complex ($\mathbf{8}^{+\bullet}$) to yield $\mathbf{A1}^{+\bullet}$ and its neutral counterpart, 5-acetoxymethyloxol-2-en-4-one (**9**). It is noteworthy that the overall dissociation energy to produce $\mathbf{A1}^{+\bullet}$, acetone, and **9** from $\mathbf{2}^{+\bullet}$ (178 kJ mol^{-1}) was notably lower than that for neutral **A1**, acetone, and $\mathbf{9}^{+\bullet}$ (316 kJ mol^{-1}), which was consistent with the absence of ion $\mathbf{9}^{+\bullet}$ (m/z 156) in the Figure 2 spectra.

The suggested mechanism pointed out the role of the dioxolane ring dissociation to steer the radical site to C2′ where it was in a position suitable for C1′–N9 bond cleavage and β-elimination of $\mathbf{A1}^{+\bullet}$. This was corroborated by the CID-MS^n spectra of the unprotected 2′,3′-OH ABCV conjugate **1b** that formed $\mathbf{A1}^{+\bullet}$ much less efficiently upon multistage collisional activation. The radical cascade starting from $\mathbf{1b}^{+\bullet}$ was analogous to that from $\mathbf{1}^{+}$ leading to the intermediate cation radical at m/z 309 (Figure 3a,b). However, CID-MS^4 of this ion resulted in a cross-ring cleavage (m/z 163) while the major nucleobase ion product was protonated adenine at m/z 136 (Figure 3a,b).

The Scheme 3 activation energies may provide a clue to explain the radically different dissociations of $\mathbf{1}^{+}$ and its deprotected analogue $\mathbf{1b}^{+}$. The low $\mathbf{TS}_{3\rightarrow7}$ energy facilitates the formation of the 2′-radical in $\mathbf{7}^{+\bullet}$ which is associated with cleavage of the C2′–O bond and elimination of acetone. An analogous reaction in the 2′,3′-OH radical intermediate, such as the one shown in Figure 3c, would require a hydrogen atom migration to 2′-OH followed by loss of water. However, neutral oxygen atoms in alcohols and ethers are very poor hydrogen atom acceptors because a H atom addition would produce high-energy hypervalent oxonium radicals.[36] This may make the formation of a C2′ radical in the 2′,3′-OH intermediate energetically prohibitive, resulting in the observed competitive cross-ring cleavage (Figure 3c).

Radical Cascade Dissociations of Guanosine Conjugates and Formation of Guanine Cation Radicals. Electrospray protonation of the guanosine ABCV conjugate **10** formed ions at m/z 586 that were subjected to CID (Figure 6a–c). Dissociations proceeded by elimination of the side

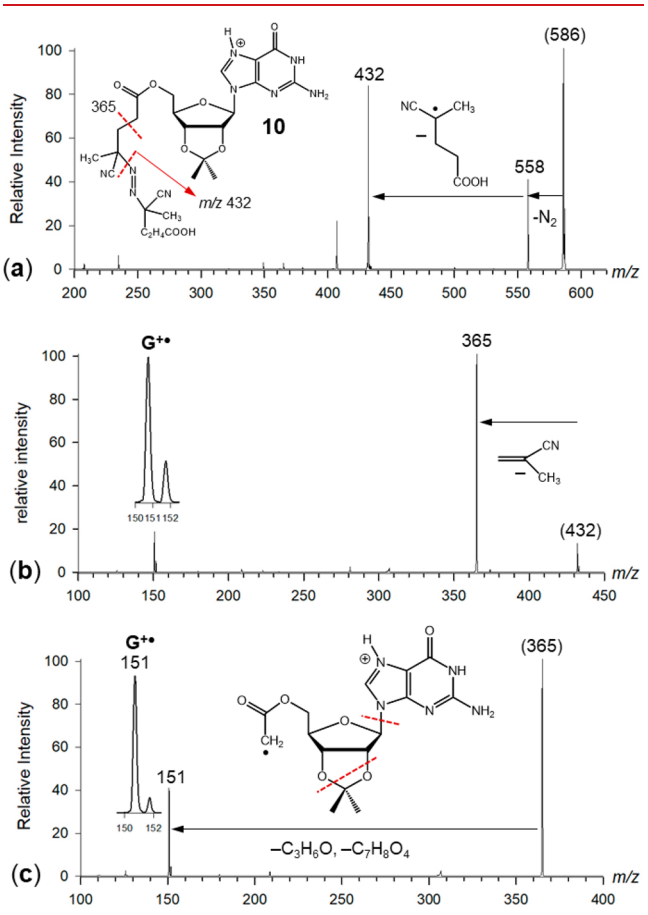

Figure 6. (a) CID-MS^2 spectrum of protonated guanosine conjugate **10** at m/z 586. (b) CID-MS^3 spectrum of fragment ion at m/z 432. (c) CID-MS^4 spectrum of fragment ion at m/z 365. Insets show the $\mathbf{G}^{+\bullet}$ and $(G + H)^+$ ion profiles at m/z 151 and 152, respectively.

chain (m/z 432, m/z 365, Figure 6a,b), followed by loss of the entire ribose moiety, forming the guanine cation radical at m/z 151 ($\mathbf{G}^{+\bullet}$). Interestingly, the intermediate fragment ion after loss of acetone (m/z 307) was only very weakly represented in the CID-MS^4 spectrum (Figure 6c). Similar to adenosine cation radicals, CID-MS^n of the deprotected 2′,3′-OH guanosine ABCV derivative did not lead to the formation of guanine cation radicals. The spectra (Figure S33, Supporting Information) showed the formation of protonated guanine ($m/$

https://doi.org/10.1021/jasms.2c00098
J. Am. Soc. Mass Spectrom. 2022, 33, 1038–1047

z 152) in all steps involved in the radical cleavage of the ABCV side chain and ribose ring.

We further used MS^5 UV–vis action spectroscopy to characterize the $\mathbf{G}^{+\bullet}$ ion (Figure 7). The spectrum was monitored at the m/z 110 fragment ion channel for the loss of CHN_2, showing a broad band extending from 410 to 600 nm, a composite band with a maximum at 330 nm, and sharper bands with maxima at 280 and 230 nm (Figure 7a). The other observed photofragment channel at m/z 127, which showed a very similar wavelength profile, probably corresponded to a water adduct to the m/z 109 fragment ion by loss of CH_2N_2 from $\mathbf{G}^{+\bullet}$. The action spectrum of $\mathbf{G}^{+\bullet}$ was distinctly different from the previously reported spectra of the canonical guanine cation radical,[13] indicating that a new isomer was produced by the radical cascade pathway. Comparison of the action spectrum with the calculated vibronic spectra showed matching bands for the N1–H, N7–H tautomer $\mathbf{G1}^{+\bullet}$ at 215 and 280 nm, as well as broad bands extending from 390 to 600 nm (Figure 7b). However, the composite band at 330 nm showed a better match with the band in the vibronic spectrum of the N1–H, N3–H isomer $\mathbf{G2}^{+\bullet}$ (Figure 7c). Both of these isomers lacked substituents at N9, which was consistent with the cation radical formation by C1′–N9 bond cleavage in the guanosine conjugate. Ion $\mathbf{G1}^{+\bullet}$ has been reported to be only 5.6 kJ mol^{-1} less stable than the canonical isomer,[13] whereas $\mathbf{G2}^{+\bullet}$ is a high-energy isomer at 75 kJ mol^{-1} above $\mathbf{G1}^{+\bullet}$. The formation of $\mathbf{G2}^{+\bullet}$ may be allowed by N3 protonation in the 5′-*O*-acetyl radical which according to our calculations was only 25 kJ mol^{-1} less favorable than protonation at N7 and thus can possibly compete to form the N3–H protomer as a minor coproduct.

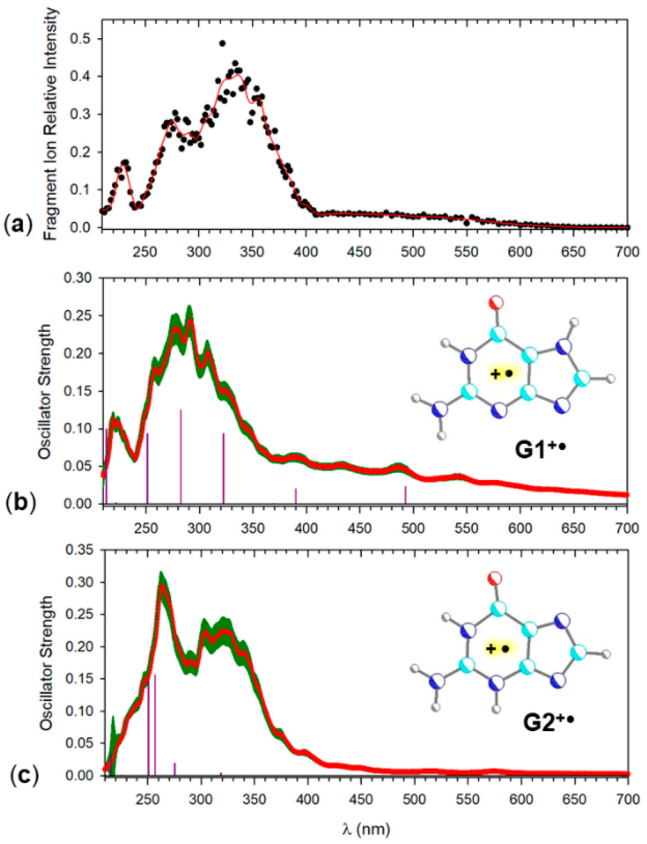

Figure 7. (a) UV–vis action spectrum of $\mathbf{G}^{+\bullet}$. M06-2X/6-31+G(d,p) calculated vibronic spectra of (b) $\mathbf{G1}^{+\bullet}$ and (c) $\mathbf{G2}^{+\bullet}$ from 300 configurations at 350 K. The vertical lines indicate TD-DFT electron transitions.

We used DFT calculations to elucidate the facile formation of $\mathbf{G1}^{+\bullet}$ upon CID. Two possible pathways to $\mathbf{G1}^{+\bullet}$ were identified, starting from the guanosine 5′-*O*-acetyl radical $\mathbf{11}^{+\bullet}$ (Scheme 4). Migration of H3′ on the acetyl radical in $\mathbf{11}^{+\bullet}$ was calculated to proceed with a TS energy of 141 kJ mol^{-1} in $\mathbf{TS}_{11\rightarrow12}$, forming the C3′ radical $\mathbf{12}^{+\bullet}$ at 7.3 kJ mol^{-1} relative to $\mathbf{11}^{+\bullet}$. However, migration of H2′ on the acetyl radical in $\mathbf{11}^{+\bullet}$ had a markedly lower TS energy (103 kJ mol^{-1} in $\mathbf{TS}_{11\rightarrow13}$) to form the C2′ radical $\mathbf{13}^{+\bullet}$ at 13 kJ mol^{-1} relative to $\mathbf{11}^{+\bullet}$. Dissociation of the C1′–N9 bond in $\mathbf{13}^{+\bullet}$ had a threshold at 187 kJ mol^{-1} forming $\mathbf{G1}^{+\bullet}$ and the neutral ribose fragment **14**. The possibility of two pathways could explain the

Scheme 4. Radical Dissociations Forming Ion $\mathbf{G1}^{+\bullet}$[a]

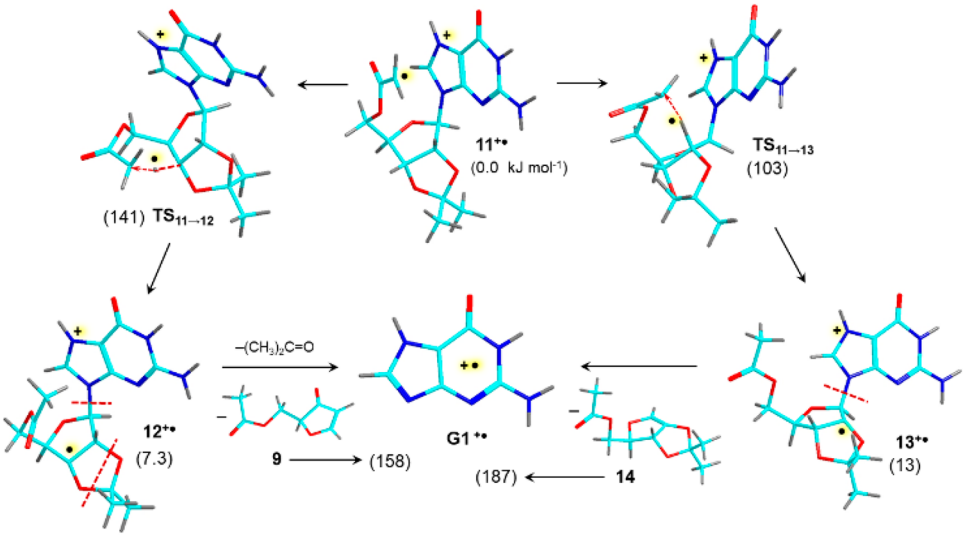

[a]Structure and energy description as in Scheme 2.

https://doi.org/10.1021/jasms.2c00098
J. Am. Soc. Mass Spectrom. 2022, 33, 1038–1047

spontaneous formation of $\mathbf{G1}^{+\bullet}$ from the 5′-acetoxy radical intermediate upon CID (Figure 6c).

Radical Cascade Dissociations of Cytidine Conjugates. CID of the protonated cytidine ABCV conjugate (m/z 546) proceeded by the expected cleavage of the radical initiator side chain, forming intermediate cation radicals at m/z 518 and 392 (Figure 8a). Upon CID-MS^2 and MS^3, we

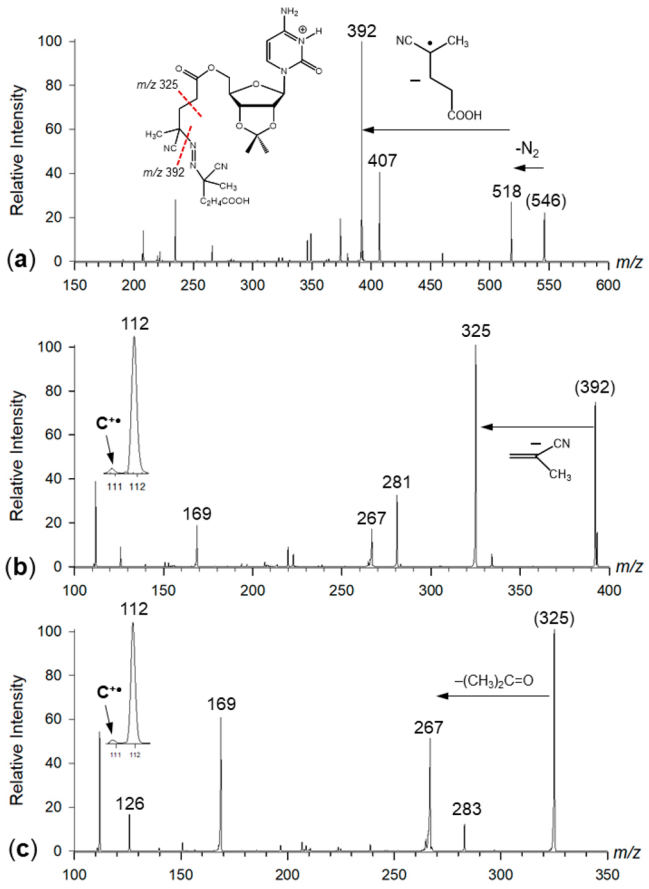

Figure 8. (a) CID-MS^2 spectrum of protonated cytidine conjugate at m/z 546. (b) CID-MS^3 spectrum of fragment ion at m/z 392. (c) CID-MS^4 spectrum of fragment ion at m/z 325. Insets show the $\mathbf{C}^{+\bullet}$ and $(C + H)^+$ ion profiles at m/z 111 and 112, respectively.

observed the respective formations of the 5′-*O*-acetyl radical ion (m/z 325) and the next generation fragment ion by loss of acetone (m/z 267). Interestingly, the CID-MS^2 spectrum in Figure 8a showed a fragment ion at m/z 407 which corresponded to loss of neutral cytosine from the $(M - N_2)$ ion at m/z 518, indicating recombination of the 2-methylglutaronitrile radical with the complementary cation radical after N_2 loss. However, subsequent dissociations of the intermediate cation radicals led to the formation of protonated cytosine cation (m/z 112), whereas the desired cytosine cation radical (m/z 111) was formed as a very minor byproduct (Figure 8b,c). We investigated another pathway to radical intermediates which was based on UV photodissociation (UVPD) of a protonated 5′-*O*-iodoacetyl conjugate of cytidine to generate radicals according to the method developed by Julian and co-workers.[37] Photodissociation at 265 nm was selected on the basis of the UV absorption spectrum of iodoacetamide which shows a broad absorption maximum at 265 nm.[38] The high excitation energy upon photon absorption (4.68 eV at 265 nm) was expected to promote C1′−N bond homolysis and formation of the desired cytosine cation radical at m/z 111. UVPD produced the 5′-*O*-acetyl radical ion a m/z 325 along with a fragment ion at m/z 341 by loss of neutral cytosine (Figure S34, Supporting Information). However, despite the high excitation upon UV photon absorption, the UVPD spectrum showed a direct and abundant formation of protonated cytosine at m/z 112, indicating again a dominant proton transfer accompanying the C1′−N bond cleavage (Scheme 5).

Scheme 5. Photodissociation of the Protected Cytidine 5′-*O*-Iodoacetyl Conjugate

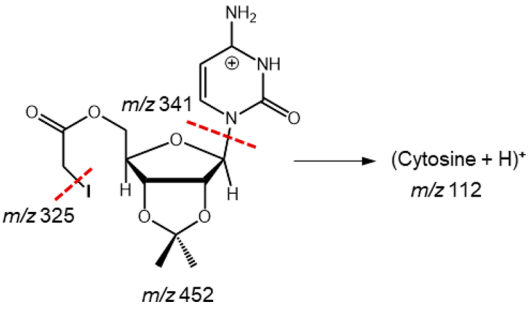

It should be noted that protonated cytosine has an intense absorption band at 231−268 nm in the gas phase, as established by action spectroscopy.[39] It is therefore possible that photodissociation of the protonated 5′-*O*-iodoacetylcytidine ion is triggered by electronic excitation in the cytosine π-electron system, driving proton transfer and elimination of protonated cytosine.

Mechanism of Cytidine Cation-Radical Dissociations. To explain the divergent behavior of cytidine conjugates, we investigated the potential energy profile of the cytidine cation radical dissociations, as shown in Scheme 6. This revealed a standard pathway starting from the 5′-*O*-acetyl radical $\mathbf{15}^{+\bullet}$ undergoing a facile H3′ transfer via $\mathbf{TS}_{15\rightarrow16}$ that was 15 kJ mol^{-1} exergonic and was followed by loss of acetone from the C3′ radical intermediate $\mathbf{16}^{+\bullet}$. However, the dissociation of the C1′−N9 bond in the critical C2′-radical intermediate $\mathbf{17}^{+\bullet}$ was substantially endergonic (ΔH_0 = 186 kJ mol^{-1}) to form the cytosine ion $\mathbf{19}^{+\bullet}$. A more facile pathway was found that proceeded via a complex of the cytosine cation radical with the ribose neutral fragment ($\mathbf{18}^{+\bullet}$). Rather than separating to the components at 203 kJ mol^{-1} threshold energy, complex $\mathbf{18}^{+\bullet}$ can undergo a hydrogen transfer to cytosine via $\mathbf{TS}_{18\rightarrow20}$ at 161 kJ mol^{-1}, forming the very stable complex $\mathbf{20}^{+\bullet}$ of protonated cytosine $\mathbf{21}^{+\bullet}$ and ribose radical $\mathbf{22}^{\bullet}$. Complex $\mathbf{20}^{+\bullet}$ was at −76 kJ mol^{-1} relative to radical $\mathbf{15}^{+\bullet}$, preventing a reversible formation of $\mathbf{18}^{+\bullet}$ and enabling dissociation to its components at a very low overall threshold energy (81 kJ mol^{-1}, Scheme 6). This reaction sequence, involving a stable intermediate ($\mathbf{20}^{+\bullet}$) and a low threshold energy, may explain the formation of protonated cytosine instead of cation radical $\mathbf{19}^{+\bullet}$.

It may be noted that the adiabatic recombination energy of the cytosine tautomer ion $\mathbf{19}^{+\bullet}$ (calculated as an absolute value of $|RE_{ad}|$ = 8.42 eV by M06-2X/6-311++G(2d,p)) was lower than the adiabatic ionization energy of fragment **9** (9.55 eV), so an electron-transfer equilibrium between those two fragments would favor ion $\mathbf{19}^{+\bullet}$. The preferential formation of protonated cytosine $\mathbf{21}^{+}$ and neutral radical $\mathbf{22}^{\bullet}$ was due to

https://doi.org/10.1021/jasms.2c00098
J. Am. Soc. Mass Spectrom. 2022, 33, 1038−1047

Scheme 6. Dissociations of the Protected Cytidine 5′-*O*-Acetyl Radical[a]

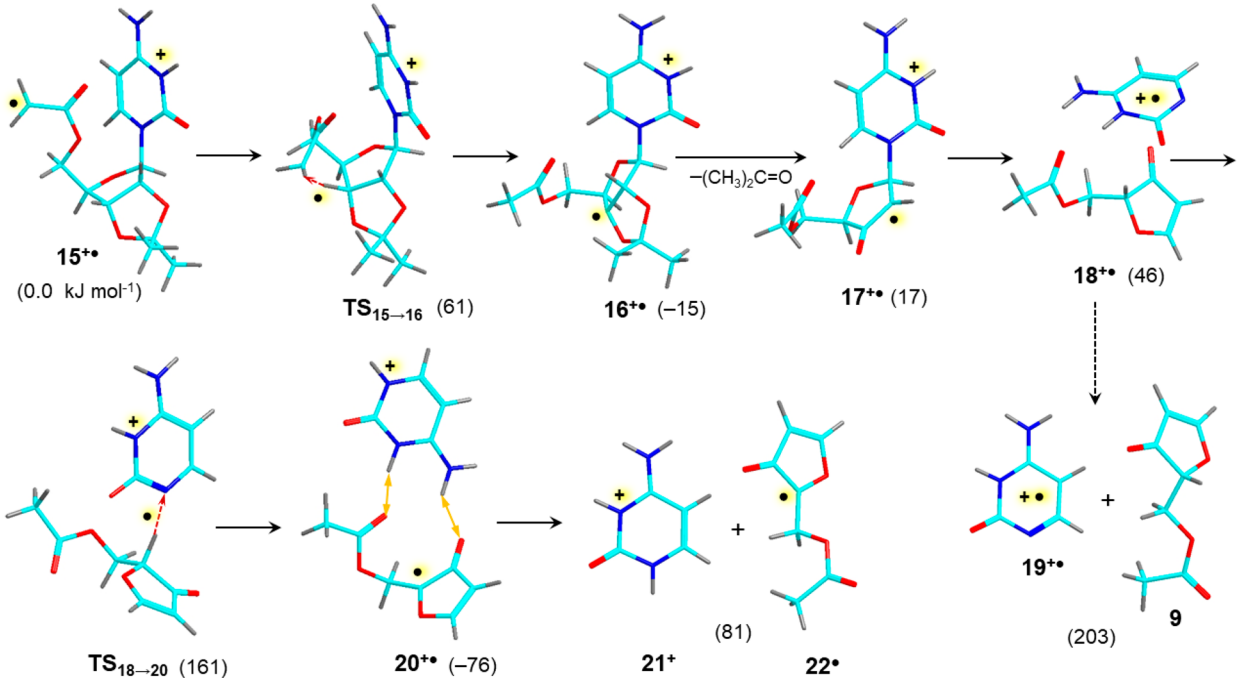

[a]Structure and energy description as in Scheme 2.

Scheme 7. Dissociations of Thymidine Conjugates upon Collisional Activation (23$^+$, left panel) and Photoexcitation at 265 nm (24$^+$, right panel)

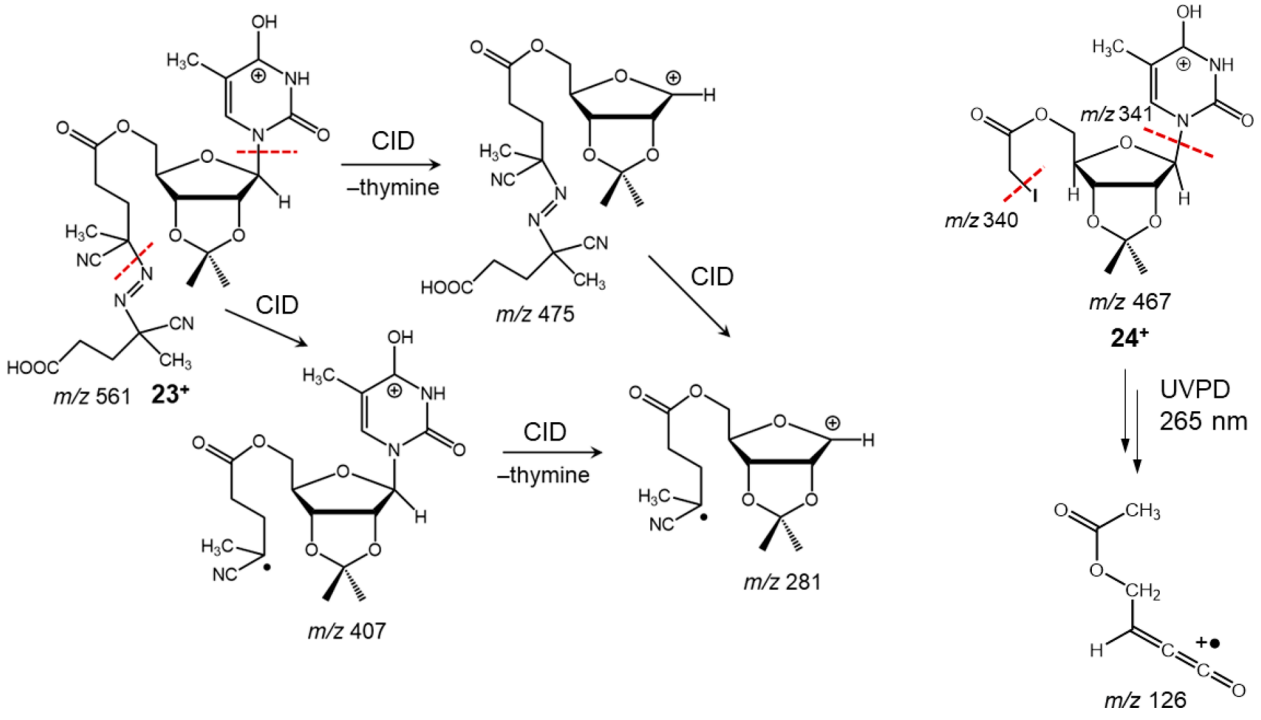

the more favorable thermodynamics for this dissociation channel.

Dissociations of Thymidine Conjugates. CID and UVPD spectra were also investigated for the 5′-*O*-ABCV and -iodoacetyl conjugates of 2′,3′-*O*-isopropylidene thymidine, respectively (Scheme 7). The CID spectra showed substantial deviations from those of its adenosine, guanosine, and cytidine analogues. The CID-MS^2 spectrum of protonated thymidine ABCV conjugate (m/z 561, **23**$^+$) showed dominant peaks for loss of thymine (m/z 475, 281, Figure S35, Supporting Information), which was also the major dissociation in the CID-MS^n spectra of the intermediates, whereas no thymine cation radicals were formed. UVPD at 265 nm of the protonated 5′-O iodoacetyl thymine conjugate (**24**$^+$, m/z 467, Figure S36a, Supporting Information) showed competitive loss of iodine (m/z 340) and thymine (m/z 341). The

https://doi.org/10.1021/jasms.2c00098
J. Am. Soc. Mass Spectrom. 2022, 33, 1038−1047

spectrum also showed fragment ions at m/z 127 for protonated thymine, and m/z 126, the latter indicating potential formation of a thymine cation radical. However, CID-MS^3 of the m/z 126 ion (Figure S36b, Supporting Information) displayed a major loss of CH_3 which is absent in the reference electron ionization spectra of thymine and its isomers.[40] We tentatively assigned the m/z 126 ion to a cumulene cation radical produced by dissociation of the ribose ring (Scheme 7).

It may be noted that thymine has a substantially lower proton affinity than the other DNA nucleobases.[40] This makes the protonated thymine ring a better leaving group than the other protonated nucleobases for cleaving the C1′−N bond and loss of the neutral nucleobase.

CONCLUSIONS

In summary, the nonredox radical cascade pathway to nucleobase cation radicals was successfully applied to generate novel isomers of adenine and guanine cation radicals which are inaccessible by direct or transition-metal-mediated ionization of standard nucleobases. The ion yields achieved in radical cascade dissociations were sufficient enough to allow us to obtain UV−vis action spectra and assign ion structures. Although radical dissociations of unprotected 2′,3′-OH conjugates did not produce nucleobase cation radicals, they did form noncanonical ribonucleoside cation radicals in which the radical and charge sites were separated. Such intermediates are of interest in studies of DNA damage[41−43] and are the subject of ongoing investigations. The formation of cytidine cation radicals was only marginal for reasons revealed by energy analysis of the radical dissociations. A radical pathway to cytosine cation radicals may benefit from photodissociation of conjugates in which the ribose moiety was modified to bypass hydrogen migration in the last step of the dissociation cascade. To this end, additional initiators are being developed that utilize electron-transfer dissociation of fixed-charge groups to form transient radical intermediates[44] and thus provide new synthetic methods for nucleoside and nucleotide cation radical generation. Generation of thymine cation radicals remains a challenge and may require a yet different approach, analogous to that used in solution studies,[45] in order to be successful in the gas phase.

ASSOCIATED CONTENT

Supporting Information

The Supporting Information is available free of charge at https://pubs.acs.org/doi/10.1021/jasms.2c00098.

Description of synthetic procedures with compound spectroscopic characterization, additional figures including NMR and mass spectra, reaction schemes and energies from DFT calculations (PDF)

AUTHOR INFORMATION

Corresponding Author

František Tureček − *Department of Chemistry, Bagley Hall, Box 351700, University of Washington, Seattle, Washington 981195-1700, United States;* orcid.org/0000-0001-7321-7858; Phone: +1-206-685-2041; Email: turecek@uw.edu

Authors

Václav Zima − *Department of Chemistry, Bagley Hall, Box 351700, University of Washington, Seattle, Washington 981195-1700, United States*

Yue Liu − *Department of Chemistry, Bagley Hall, Box 351700, University of Washington, Seattle, Washington 981195-1700, United States*

Complete contact information is available at: https://pubs.acs.org/10.1021/jasms.2c00098

Notes

The authors declare no competing financial interest.

ACKNOWLEDGMENTS

Support by the Chemistry Division of the U.S. National Science Foundation (grant CHE-1951518) and the Klaus and Mary Ann Saegebarth Endowment is gratefully acknowledged.

REFERENCES

(1) von Sonntag, C. Free-Radical-Induced DNA Damage as Approached by Quantum-Mechanical and Monte Carlo Calculations: An Overview from the Standpoint of an Experimentalist. In *Advances in Quantum Chemistry*; Sabin, J. R., Brändas, E., Eds.; Academic Press, 2007; Vol. *52*, pp 5−20.

(2) Giese, B. Long-Distance Electron Transfer Through DNA. *Annu. Rev. Biochem.* **2002**, *71*, 51−70.

(3) Wagenknecht, H.-A.; Fiebig, T. *Charge Transfer in DNA*; John Wiley & Sons, Ltd, 2005.

(4) Douki, T.; Ravanat, J.-L.; Angelov, D.; Wagner, J. R.; Cadet, J. Effects of Duplex Stability on Charge-Transfer Efficiency within DNA. In *Long-Range Charge Transfer in DNA I*; Schuster, G. B., Ed.; Springer: Berlin, 2004; pp 1−25.

(5) Kawai, K.; Majima, T. Hole Transfer Kinetics of DNA. *Acc. Chem. Res.* **2013**, *46*, 2616−2625.

(6) Boudaïffa, B.; Cloutier, P.; Hunting, D.; Huels, M. A.; Sanche, L. Resonant Formation of DNA Strand Breaks by Low-Energy (3 to 20 eV) Electrons. *Science* **2000**, *287*, 1658−1660.

(7) Tureček, F. Flying DNA Cation Radicals in the Gas Phase: Generation and Action Spectroscopy of Canonical and Noncanonical Nucleobase Forms. *J. Phys. Chem. B* **2021**, *125*, 7090−7100.

(8) Antoine, R.; Dugourd, P. UV-Visible Activation of Biomolecular Ions. In *Laser Photodissociation and Spectroscopy of Mass-separated Biomolecular Ions*; Polfer, N. C., Dugourd, P., Eds.; Springer International Publishing: Cham, 2013; pp 93−116.

(9) Wee, S.; O'Hair, R. A. J.; McFadyen, W. D. Can Radical Cations of the Constituents of Nucleic Acids Be Formed in the Gas Phase Using Ternary Transition Metal Complexes? *Rapid Commun. Mass Spectrom.* **2005**, *19*, 1797−1805.

(10) Lam, A. K. Y.; Abrahams, B. F.; Grannas, M. J.; McFadyen, W. D.; O'Hair, R. A. J. Tuning the Gas Phase Redox Properties of Copper(II) Ternary Complexes of Terpyridines to Control the Formation of Nucleobase Radical Cations. *Dalton Trans.* **2006**, No. 42, 5051−5061.

(11) Huang, S. R.; Tureček, F. Cation Radicals of Hachimoji Nucleobases. Canonical Purine and Noncanonical Pyrimidine Forms Generated in the Gas Phase and Characterized by UV−Vis Photodissociation Action Spectroscopy. *J. Phys. Chem. A* **2020**, *124*, 7101−7112.

(12) Feketeová, L.; Chan, B.; Khairallah, G. N.; Steinmetz, V.; Maître, P.; Radom, L.; O'Hair, R. A. J. Gas-Phase Structure and Reactivity of the Keto Tautomer of the Deoxyguanosine Radical Cation. *Phys. Chem. Chem. Phys.* **2015**, *17*, 25837−25844.

(13) Dang, A.; Liu, Y.; Tureček, F. UV-Vis Action Spectroscopy of Guanine, 9-Methylguanine and 2′-Deoxyguanosine Cation Radicals in the Gas Phase. *J. Phys. Chem. A* **2019**, *123*, 3272−3284.

(14) Liu, Y.; Dang, A.; Urban, J.; Tureček, F. Charge-Tagged DNA Radicals in the Gas Phase Characterized by UV-Vis Photodissociation

Action Spectroscopy. *Angew. Chem., Int. Ed. Engl.* **2020**, *59*, 7772−7777.
(15) Huang, S. R.; Liu, Y.; Tureček, F. UV-Vis Photodissociation Action Spectroscopy Reveals Cytosine-Guanine Hydrogen Transfer in DNA Tetranucleotide Cation Radicals upon One-Electron Reduction. *J. Phys. Chem. B* **2020**, *124*, 3505−3517.
(16) Liu, Y.; Huang, S. R.; Tureček, F. Guanine-Adenine Interactions in DNA Tetranucleotide Cation Radicals Revealed by UV/Vis Photodissociation Action Spectroscopy and Theory. *Phys. Chem. Chem. Phys.* **2020**, *22*, 16831−16842.
(17) Hodyss, R.; Cox, H. A.; Beauchamp, J. L. Bioconjugates for Tunable Peptide Fragmentation: Free Radical Initiated Peptide Sequencing (FRIPS). *J. Am. Chem. Soc.* **2005**, *127*, 12436−12437.
(18) Desai, N.; Thomas, D. A.; Lee, J.; Gao, J.; Beauchamp, J. L. Eradicating Mass Spectrometric Glycan Rearrangement by Utilizing Free Radicals. *Chem. Sci.* **2016**, *7*, 5390−5397.
(19) Dang, A.; Korn, J. A.; Gladden, J.; Mozzone, B.; Turecek, F. UV-Vis Photodissociation Action Spectroscopy on Thermo LTQ-XL ETD and Bruker amaZon Ion Trap Mass Spectrometers: A Practical Guide. *J. Am. Soc. Mass Spectrom.* **2019**, *30*, 1558−1564.
(20) Liu, Y.; Turecek, F. Photodissociative Crosslinking of Diazirine-Tagged Peptides with DNA Dinucleotides in the Gas Phase. *J. Am. Soc. Mass Spectrom.* **2019**, *30*, 1992−2006.
(21) Berendsen, H. J.; Postma, J. V.; van Gunsteren, W. F.; DiNola, A. R. H. J.; Haak, J. R. Molecular Dynamics with Coupling to an External Bath. *J. Chem. Phys.* **1984**, *81*, 3684−3690.
(22) Řezáč, J.; Fanfrlík, J.; Salahub, D.; Hobza, P. Semi-Empirical Quantum Chemical PM6 Method Augmented by Dispersion and H Bonding Correction Terms Reliably Describes Various Types of Noncovalent Complexes. *J. Chem. Theory Comput.* **2009**, *5*, 1749−1760.
(23) Stewart, J. J. P. *MOPAC 16. Stewart Computational Chemistry*; Colorado Springs, CO, 2016.
(24) Řezáč, J. Cuby: An Integrative Framework for Computational Chemistry. *J. Comput. Chem.* **2016**, *37*, 1230−1237.
(25) Becke, A. D. Density-Functional Exchange-Energy Approximation with Correct Asymptotic Behavior. *Phys. Rev. A* **1988**, *38*, 3098−3100.
(26) Zhao, Y.; Truhlar, D. G. The M06 Suite of Density Functionals for Main Group Thermochemistry, Thermochemical Kinetics, Noncovalent Interactions, Excited States, and Transition Elements: Two New Functionals and Systematic Testing of Four M06-Class Functionals and 12 Other Functionals. *Theor. Chem. Acc.* **2008**, *120*, 215−241.
(27) Frisch, M. J.; Trucks, G. W.; Schlegel, H. B.; Scuseria, G. E.; Robb, M. A.; Cheeseman, J. R.; Scalmani, G.; Barone, V.; Petersson, G. A.; Nakatsuji, H.; Caricato, M.; Marenich, A. V.; Bloino, J.; Janesko, B. G.; Gomperts, R.; Mennucci, B.; Hratchian, H. P.; Ortiz, J. V.; Izmaylov, A. F.; Sonnenberg, J. L.; Williams-Young, D.; Ding, F.; Lipparini, F.; Egidi, F.; Goings, J.; Peng, B.; Petrone, A.; Henderson, T.; Ranasinghe, D.; Zakrzewski, V. G.; Gao, J.; Rega, N.; Zheng, G.; Liang, W.; Hada, M.; Ehara, M.; Toyota, K.; Fukuda, R.; Hasegawa, J.; Ishida, M.; Nakajima, T.; Honda, Y.; Kitao, O.; Nakai, H.; Vreven, T.; Throssell, K.; Montgomery, J. A., Jr.; Peralta, J. E.; Ogliaro, F.; Bearpark, M. J.; Heyd, J. J.; Brothers, E. N.; Kudin, K. N.; Staroverov, V. N.; Keith, T. A.; Kobayashi, R.; Normand, J.; Raghavachari, K.; Rendell, A. P.; Burant, J. C.; Iyengar, S. S.; Tomasi, J.; Cossi, M.; Millam, J. M.; Klene, M.; Adamo, C.; Cammi, R.; Ochterski, J. W.; Martin, R. L.; Morokuma, K.; Farkas, O.; Foresman, J. B.; Fox, D. J. *Gaussian 16, revision A01*; Gaussian, Inc., Wallingford, CT, 2016.
(28) Polfer, N.; Sartakov, B. G.; Oomens, J. The Infrared Spectrum of the Adamantyl Cation. *Chem. Phys. Lett.* **2004**, *400*, 201−205.
(29) Furche, F.; Ahlrichs, R. Adiabatic Time-Dependent Density Functional Methods for Excited State Properties. *J. Chem. Phys.* **2002**, *117*, 7433−7447.
(30) Wigner, E. On The Quantum Correction for Thermodynamic Equilibrium. *Phys. Rev.* **1932**, *40*, 749−759.
(31) Bonačić-Koutecký, V.; Mitrić, R. Theoretical Exploration of Ultrafast Dynamics in Atomic Clusters: Analysis and Control. *Chem. Rev.* **2005**, *105*, 11−66.
(32) Barbatti, M.; Ruckenbauer, M.; Plasser, F.; Pittner, J.; Granucci, G.; Persico, M.; Lischka, H. Newton-X: A Surface-Hopping Program for Nonadiabatic Molecular Dynamics. Wiley Interdisciplinary Reviews. *Comput. Mol. Sci.* **2014**, *4*, 26−33.
(33) Huang, S. R.; Dang, A.; Tureček, F. Ground and Excited States of Gas-Phase DNA Nucleobase Cation-Radicals. A UV-Vis Photodisociation Action Spectroscopy and Computational Study of Adenine and 9-Methyladenine. *J. Am. Soc. Mass Spectrom.* **2020**, *31*, 1271−1281.
(34) Huang, S. R.; Nováková, G.; Marek, A.; Tureček, F. The Elusive Non-Canonical Isomers of Ionized 9-Methyladenine and 2′-Deoxyadenosine. *J. Phys. Chem. A* **2021**, *125*, 338−348.
(35) Wu, R. R.; Yang, B.; Berden, G.; Oomens, J.; Rodgers, M. T. Gas-Phase Conformations and Energetics of Protonated 2′-Deoxyadenosine and Adenosine: IRMPD Action Spectroscopy and Theoretical Studies. *J. Phys. Chem. B* **2015**, *119*, 2795−2805.
(36) Tureček, F.; Reid, P. J. Metastable States of Dimethyloxonium, $(CH_3)_2OH^{\bullet}$. *Int. J. Mass Spectrom.* **2003**, *222*, 49−61.
(37) Ly, T.; Julian, R. R. Residue-Specific Radical-Directed Dissociation of Whole Proteins in the Gas Phase. *J. Am. Chem. Soc.* **2008**, *130*, 351−358.
(38) Finkle, B. J.; Smith, E. L. Crystalline Papain: Number and Reactivity of Thiol Groups; Chromatographic Behavior. *J. Biol. Chem.* **1958**, *230*, 669−690.
(39) Berdakin, M.; Féraud, C.; Dedonder-Lardeux, C.; Jouvet, C.; Pino, G. A. Excited States of DNA/RNA Bases. *Phys. Chem. Chem. Phys.* **2014**, *16*, 10643−10650.
(40) NIST Chemistry Webbook, Standard Reference Database Number 69; https://webbook.nist.gov/chemistry. Accessed March 2022.
(41) Kumar, A.; Pottiboyina, V.; Sevilla, M. D. One-Electron Oxidation of Neutral Sugar Radicals of 2′-Deoxyguanosine and 2′-Deoxythymidine: A Density Functional Theory (DFT) Study. *J. Phys. Chem. B* **2012**, *116*, 9409−9416.
(42) Adhikary, A.; Collins, S.; Khanduri, D.; Sevilla, M. D. Sugar Radicals Formed by Photoexcitation of Guanine Cation Radical in Oligonucleotides. *J. Phys. Chem. B* **2007**, *111*, 7415−7421.
(43) Kumar, A.; Sevilla, M. D. Sugar Radical Formation by a Proton Coupled Hole Transfer in 2′-Deoxyguanosine Radical cation (2′-$dG^{\bullet+}$): A Theoretical Treatment. *J. Phys. Chem. B* **2009**, *113*, 13374−13380.
(44) Zimnicka, M.; Moss, C. L.; Chung, T. W.; Hui, R.; Tureček, F. Tunable Charge Tags for Electron-Based Methods of Peptide Sequencing: Design and Applications. *J. Am. Soc. Mass Spectrom.* **2012**, *23*, 608−620.
(45) Sun, H.; Taverna Porro, M. L.; Greenberg, M. M. Independent Generation and Reactivity of Thymidine Radical Cations. *J. Org. Chem.* **2017**, *82*, 11072−11083.

https://doi.org/10.1021/jasms.2c00098
J. Am. Soc. Mass Spectrom. 2022, 33, 1038−1047